

Adrienne R. Minerick  
Agnes E. Ostafin  
Hsueh-Chia Chang

Department of  
Chemical Engineering,  
University of Notre Dame,  
Notre Dame, IN, USA

## Electrokinetic transport of red blood cells in microcapillaries

Electrokinetic flow of a suspension of erythrocytes (red blood cells, RBCs) in 20  $\mu\text{m}$  cylindrical fused-silica capillaries is examined in the present work. Flow direction anomalies are observed experimentally and tentatively explained by the development of a pH gradient between the cathode well and the anode well due to electrolysis reactions at the electrodes. This pH gradient alters the local zeta potentials of both the capillary and the RBC and thus the local electroendosmotic liquid flow (EOF) velocities and RBC electrophoretic (EP) velocities. The two velocities are opposite in direction but with EOF dominating such that the RBC moves toward the cathode, opposite to the anode migration observed in bulk conditions. The opposing zeta potentials also lead to RBC aggregation at the anode end for low fields less than 25 V/cm. As the electroendosmotic velocity decreases at the anode end due to decreasing pH, pressure-driven back flow develops to oppose the original EOF at the remaining portions of the capillary ensuring constant fluid flux. When the anode EOF velocity is smaller in magnitude than the EP velocity, reversal of blood cell transport is observed after a short transient time in which a pH gradient forms. RBC velocities and pH dependencies on electric field and  $\text{MgCl}_2$  concentration are presented along with data showing the accumulation of charge separation across the capillary. Also, a short-term solution to the pH gradient formation is presented that could help thwart development of pH gradients in micro-devices at lower voltages.

**Keywords:** Electrokinetic flow / Erythrocyte / pH gradient / Microfluidic device / Zeta potential

EL 5016

### 1 Introduction

The possibility of transporting erythrocytes and proteins through microcapillaries with longitudinal electric fields has great potential in the development and fabrication of the next generation of chip-based miniaturized medical diagnostic kits for patient/drug selection, infectious disease, cellular anomalies, sickle cell characteristics, and other blood related medical problems. Such problems are currently tested for with more time-consuming 96-well plate screening methods, microscopy, or by reagent strip technologies and require relatively large volumes of blood.

Current chip-based microfluidic devices rely on electrokinetic flow to transport reactants, products and waste in rectangular channels [1]. Transporting bubbles, nonelectrolyte liquid drops, and blood cells in microchannels of comparable dimension remains problematic [2, 3]. Nevertheless, it is envisioned that in the near future, entire laboratory pro-

cesses ranging from very selective separations to single cell analysis will be incorporated on a chip [4]. So far, limited work has been done in the development of microscale devices for the direct analysis of the cellular components of blood. The biconcave shape and structure variation typical of RBCs, as well as their dependence on solvent conditions, pH, tonicity, and temperature create added complications in the transport of RBCs in microchannels.

Electrokinetic fluid movement of cells in microchannels is strongly influenced by the cell surface charge, but is still expected to follow the same rules of movement as less complicated, charged colloidal objects in electric fields [4–7]. The erythrocytes are transported both electrophoretically due to their surface charges (proteins in the membrane adjust with tonicity of the buffer solution [8]) and convectively by the EOF of the electrolyte in the buffer solution interacting with the fused-silica capillary wall [5–7]. However, the cellular surface charge and topography may also be influenced by local changes on the capillary walls, local gradients in pH, tonicity, and chemical composition of the fluid in the capillary, which then changes the movement of the cells. Much work has been done with pressure-driven flow where dilute concentrations of erythrocytes are observed to favor the capillary axis [9–11]. Cells are found to settle gravitationally in pressure-driven flows of RBC suspensions [9–11].

**Correspondence:** Dr. Hsueh-Chia Chang, Department of Chemical Engineering, University of Notre Dame, 182 Fitzpatrick, Notre Dame, IN, USA 46556  
**E-mail:** chang.2@nd.edu  
**Fax:** +219-631-8366

**Abbreviations:** **EP**, electrophoretic; **RBC**, red blood cells (erythrocytes)

In the current work, we report additional flow anomalies associated with electrokinetic RBC transport in microchannels. It is known from prior work that the zeta potential of RBC in phosphate-buffered saline (PBS) is positive such that it migrates electrophoretically toward the anode in a bulk electrolyte or in a large capillary [5]. However, when we drive them electrokinetically through a 20  $\mu\text{m}$  inside diameter (ID) cylindrical fused-silica capillary, RBCs first travel toward the cathode. After a transient period ranging from about 30 min to 15 h, depending on the electric field, RBC movement is observed heading in the direction of the anode. During this period of time, a substantial pH gradient across the capillary develops from a neutral 7.4 everywhere to as high as 12 in the cathode well and as low as 2 in the anode well. Such flow behaviors suggest either a change in EOF governed by the capillary surface charge, or an increase in the charge distribution of proteins within the RBC membrane such that electrophoretic motion towards the anode is so enhanced that it overcomes the opposite electroendosmotic velocity.

We present evidence that the observed flow reversal is due to local changes in electroendosmotic and electrophoretic velocities due to the formation of a pH gradient in the capillary from an electrolysis reaction at the electrodes [12, 13]. At the anode end of the capillary, pH drops so low that the surface charge either becomes neutral or changes sign [14]. As the EOF at the anode drops to zero or reverses, fluid flow in the direction opposing the original EOF develops in the rest of the capillary to ensure constant fluid flux. The lower pH at the anode can also increase the positive zeta potential of the RBC and increase its propensity to travel to the anode. RBC velocities and pH dependence on electric field is presented along with data showing the accumulation of charge separation across the capillary. We also outline theoretical verification of critical conditions leading to development of the pH gradient as a tentative explanation for flow reversal in our system. In lower electric fields, we are able to prevent the formation of a pH gradient by adding  $\text{MgCl}_2$  salt to the solution thus preventing flow reversal. We also show that, at low electric fields, the blood cells are attracted to the oppositely charged capillary, especially at corners where the electric field enhances the local charge density.

## 2 Materials and methods

Fresh human whole blood was obtained via venipuncture and stored in vacutainers (Becton Dickinson) containing 1.8 mg  $\text{K}_2\text{EDTA}$  per mL of blood. Whole blood components were separated by centrifugation using a Sorvall

Super T 21 Centrifuge at 3000 rpm for 15 min with a Sorvall SLC-250T Rotor at 4°C [15]. The erythrocyte portion was isolated and washed according to the procedure by Takeuchi and co-workers [15] then stored in the refrigerator at 4°C in isotonic PBS (140 mM NaCl, 22 mM  $\text{KH}_2\text{PO}_4$ , 9.1 mM  $\text{K}_2\text{HPO}_4$ ) until use [8]. Experiments are carried out in 20  $\mu\text{m}$  ID capillaries (Polymicro Technologies, Phoenix, AZ, USA) 3 cm in length with an applied voltage of 50–200 V per 4 cm. The device, with its built-in electrode reservoirs, was constructed from polycarbonate to hold 2 mL of fluid in each well. Electrodes are constructed out of 0.1 mm platinum wire (Goodfellow, Huntingdon, UK) and positioned approximately 1 mm from the opening of the capillary ends. Position of the electrode was accomplished by adjusting a Teflon screw containing a small bore hole lengthwise which houses the platinum wire. The apparatus is shown in the schematic in Fig. 1. RBC movement was visually recorded with an Olympus LM PlanFl 50X objective on a microscope equipped with a Panasonic GP-KR222 CCD camera. Digital output from the camera was routed directly to the computer with an ATI All-In-Wonder 128 video capture card and to a JVC HR-S9800U video recorder. An Accumet Calomel Combination pH/ATC electrode was immersed in each well during operation of the electrokinetic cell. The pH values were recorded in real time as a function of  $\text{MgCl}_2$  concentration and voltage using a DATEL PC 412LV data acquisition board and a LAB VIEW interface on a PC. Voltage was monitored with a Wavetek Meterman 15XL multimeter. Probes were immersed in the wells with the point of the probe centered between the platinum electrode and the end of the capillary. Voltage readings were recorded at fixed time intervals.

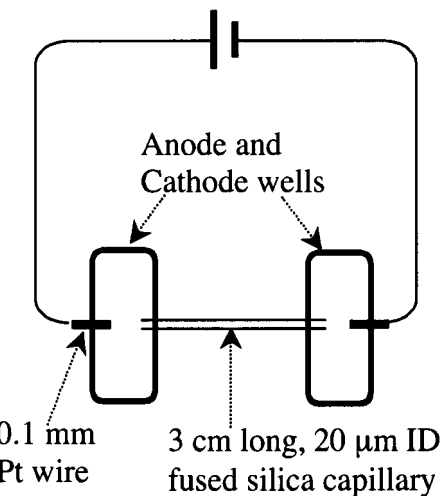


**Figure 1.** Electrokinetic capillary cell setup. The entire device is mounted on a microscope stage and video images are recorded from below.

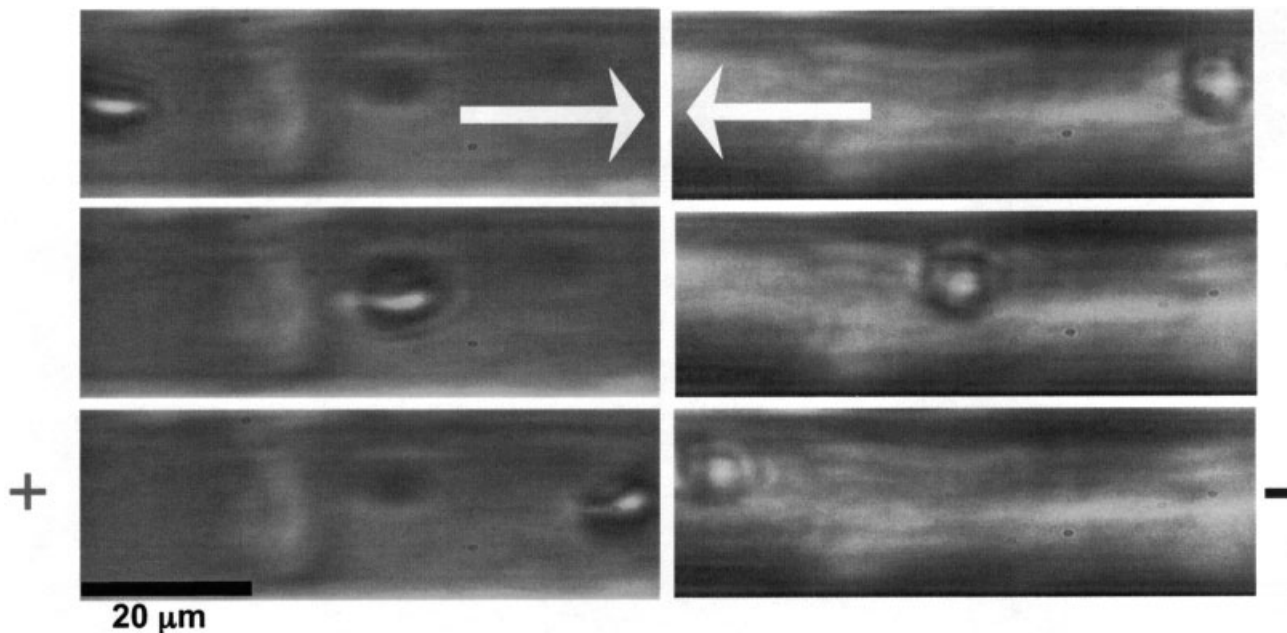


**Figure 2.** Erythrocyte movement in a 20  $\mu\text{m}$  ID fused-silica capillary. Movement is first toward the cathode, then reverses and flows toward the anode.

### 3 Results

Figure 2 shows the movement of erythrocytes in a 20  $\mu\text{m}$  ID capillary before flow reversal and after flow reversal. The wells contain 1–3 day old red blood cells (RBCs) in a suspension (10  $\mu\text{L}$  concentrated RBCs, washed and separated, to 2 mL PBS), for an electric field of 50 V/cm. The dependence of the pH of PBS (without erythrocytes present) over time on voltage is shown in Fig. 3 for the electric fields: 12.5, 25, and 37.5 V/cm. At 12.5 V/cm, the pH exhibits a large jump in the initial 10 min to eventually level out after 50 min to approximately pH 11 on the cathode side and pH 3.5 on the anode side. Data at 25 V/cm, differs slightly from this. The pH in the anode and cathode wells change only slightly in the first 10 min, but increases to then level out after 60 min, to approximately pH 10.5 in the cathode well and pH 3.4 in the anode well. However, at 37.5 V/cm, the pH in the cathode well not only jumps quickly in the first 10 min, but continues to climb to a pH of about 12.5 after 60 min. The anode well does not exhibit the jump in the first 10 min, but changes so quickly that within 40 min, the concentration of  $\text{H}^+$  is too high for the pH meter to register.

The voltage discharge across the capillary was monitored with a multimeter immediately after turning off the power supply (Fig. 4). The diamond ( $\blacklozenge$ ) and the square ( $\blacksquare$ ) are the RBC suspension in PBS after charging the PBS-loaded device for 5 h at 50 V/cm, and after a 5-min recharge following the initial discharge experiment respectively. The

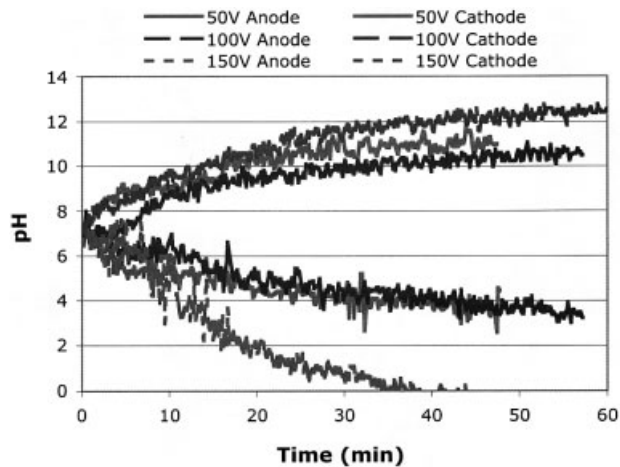


**Figure 3.** Changes in pH in the anode and cathode wells over time. Data is shown for 12.5, 25, and 37.5 V/cm.

circle ( $\bullet$ ) represents the observed voltage discharge for both wells full of deionized (E-pure), water (18 m $\Omega$ ), which was charged for 10 min at 50 V/cm. After approximately 6 h, the residual voltage offset disappears in all cases. In an attempt to prevent the formation of the pH gradient,  $\text{MgCl}_2$  was added at increasing concentrations. At fields less than 12.5 V/cm,  $\text{MgCl}_2$  prevents the formation of the pH gradient. This is shown in Fig. 5 as a function of  $\text{MgCl}_2$  concentration. A precipitate is evident at the cathode when the salt is added and increases with the concentration of  $\text{MgCl}_2$ .

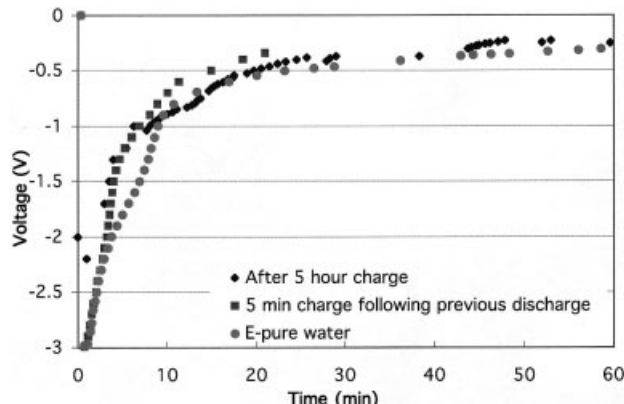


**Figure 4.** Discharge voltages for PBS with RBCs and for E-pure water. All experiments were charged in a field of 50 V/cm. There is no voltage offset before the experiment begins.

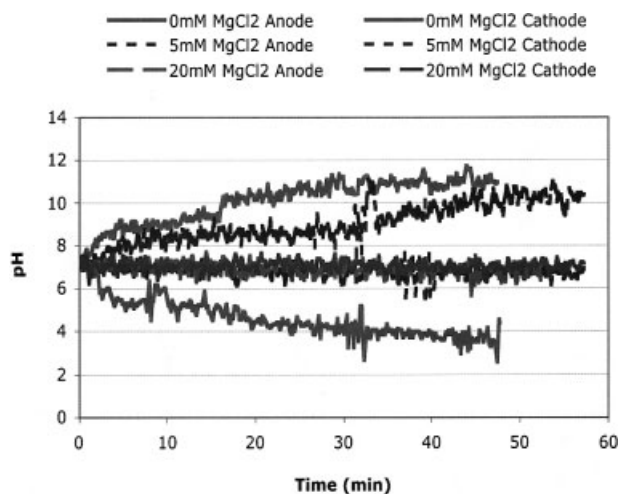


**Figure 5.** At 12.5 V/cm,  $MgCl_2$  has an impact on the development of the pH gradient over time. Higher concentrations of  $MgCl_2$  prevent the accumulation of  $H^+$  ions and  $OH^-$  ions in the anode and cathode wells, respectively.

The polarization characteristics, including time scales and potential drops, are drastically different when erythrocytes are added to the device. In addition, the RBC behaviors in the microdevice are strongly dependent on the applied electric field and the resulting polarization. In an electric field of 12.5  $\mu$ m/s, RBC velocities are initially on the order of approximately 11 V/cm, which is slow enough that gravitational settling is readily observed. Once cells have settled to the bottom of the capillary, the flow field appears altered, cells tumble (instead of translate) down the capillary and have a tendency to get caught on previously settled cells. After a period of time, a clot of cells obstructs the capillary. The system needs to be rebuilt with a fresh capillary once this occurs.



**Figure 6.** Image of the anode end of the capillary. RBCs tend to aggregate at the opening of the capillary. The development of high zeta potentials at corners in electric fields has been observed elsewhere [16].

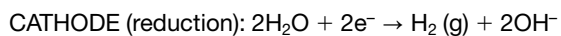
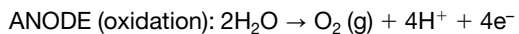
In an electric field of 25 V/cm, initial observed RBC velocities are around 21  $\mu$ m/s and gravitational settling is observed less frequently. However, a new problem begins to arise in this larger field. The cells now, tend to aggregate around the anode entrance to the capillary as is shown in Fig. 6. Eventually, the mass of cells is sucked in the end of the capillary, sealing off any flow. Decreasing the concentration of the RBC suspension slows the growth of the aggregate, but fewer cells are sucked into the capillary and less data can be obtained. This phenomenon is also observed at corners and sharp edges in electric fields even with latex beads [16].

At an electric field of 37.5 V/cm, initial RBC velocities in the system are observed to be approximately 30 m/s, while at 50 V/cm, velocities increase to about 41 m/s. Continuous observation of the system shows RBC velocities decreasing with time. After 3.5 h at 25 V/cm, RBC velocities have decreased to about 17 m/s from the initial value of 21 m/s. This is not accompanied by a significant change in pH in either well. At 12 h, velocities are at approximately 15 m/s and pH is 7.43 in the cathode well and 7.18 in the anode well. At 14.5 h, pH is still relatively steady, but within 1.5 h, cathode pH is 10.38 and anode pH is 6.00. RBCs are observed traveling toward the anode at 16 h when the pH of the cathode well is at 11.73 and the anode well is at 2.52. These pH transients are obviously much longer than the PBS without erythrocytes. Gas production at this time (an indicator of the electrolysis reaction) occurs rapidly in both wells. Interestingly, the system with the RBC suspension does not show the immediate changes in pH that the PBS system demonstrated in Fig. 3. In the experiment just described, it took a little over 15 h before either well experienced a change in pH. Once started, pH changes rapidly and seems to follow the same behavior seen in the PBS system.

#### 4 Discussion

Since settling and aggregation in the middle of the capillary occurs at low electric fields, it could be due to gravitational setting or due to DLVO type RBC attraction [17]. Both are expected to disappear at high electric fields with high hydrodynamic stress where the RBC will tend to migrate towards the middle of the axis due to deformation, finite-size effects or other hydrodynamic migration effects [9–11]. This prevents settling. The shear and the electric field also should minimize cell aggregation. We did not study these settling phenomena in detail but focused instead on flow reversal above electric fields of 12.5 V/cm. The experimental evidence indicates that the RBC transport reversal might be due to a pH gradient developing across the capillary. Voltage discharge experiments also suggest that an ion gradient could be developing in addition to the pH gradient. The polarization across the capillary is due to the production of electrons at the anode and the consumption of electrons at the cathode as well as the selective electromigration of buffer ions. This gradient and net voltage dissipates slowly over time but remains even after 1 h indicating the nonuniform loss of ion mass from both electrode wells.

Electrolysis of water at platinum electrodes occurs via oxidation/reduction reactions. The cathode reduction reaction utilizes two electrons to break apart water. This results in H<sub>2</sub> gas evolution and an increase in OH<sup>−</sup> ions within the well. The complementary oxidation reaction at the anode electrode results in O<sub>2</sub> gas formation and an accumulation of H<sup>+</sup> thus causing a shift to lower pHs. The net result is an accumulation of H<sup>+</sup> ions in the anode well and OH<sup>−</sup> in the cathode well.



However, since the pH in the erythrocyte suspension system is held constant before reaching a critical time after which pH changes rapidly, the H<sup>+</sup> and OH<sup>−</sup> ions generated initially could be absorbed by the RBC and capillary surface such that no pH change in the solution is observed. We suspect, with its larger ion capacity, the RBC absorbs most of the initial ions generated at the electrodes. This is further supported by tabulated zeta potential values for RBC [18]. The absorbed ions on the RBC could, however, increase its positive zeta potential and the electrophoretic velocity towards the anode. The enhanced electrophoretic velocity due to ion absorption is, however, still smaller than the electroendosmotic velocity towards the cathode, such that the net RBC velocity is still towards the cathode but it decreases with time.

The conclusion that erythrocytes and the fused silica capillary have opposite zeta potentials is also consistent with the aggregation that occurs at the anode end of the capillary seen in Fig. 6. If the pH remains neutral at that end, then many of the H<sup>+</sup> ions are being absorbed by the RBC. These local RBC would have the largest positive zeta potential and would most likely to be attracted to the fused-silica corner at the anode. Our other work has shown that corners at capillaries tend to have the large potentials due to field singularities in the electrostatic Laplace equation [16]. However, the RBC will eventually saturate (as long as 15 h in our experiments) and cannot absorb additional H<sup>+</sup> or OH<sup>−</sup> ions resulting in the pH at both electrodes changing sharply with the pH decreasing at the proton-generating anode. These excess protons can then absorb on to the capillary and change the electroendosmotic velocities. The absorption time onto the capillary seems to be about 1.5 h and much smaller than the RBC saturation time. This is consistent with the much lower capacitance of the capillary surface. Hence, 1.5 h after the RBC is saturated, the electroendosmotic velocity also begins to change – but it decreases in a peculiar manner.

Convective liquid flow reversal can occur due to a peculiar characteristic of unidirectional electrokinetic flow in a charged capillary. In the presence of an electric field, the electrostatic body force due to the longitudinal electric field,  $E$ , is only present within the thin polarized Debye layer (10–200 nm in thickness) on the capillary wall. As a consequence, this body force manifests itself as a surface force and is mathematically represented by the Smoluchowski slip velocity at the wall.

$$u_{\text{EOF}}(r = a) = \frac{\epsilon \zeta E}{\mu} \quad (1)$$

where the zeta potential,  $\zeta$ , the charge difference between the surface of the silica capillary and the bulk ion concentration, is the determining factor in EOF,  $u_{\text{EOF}}$  characteristics. The dielectric permittivity,  $\epsilon$ , and the viscosity,  $\mu$ , of water remain constant over all conditions in our system. In the absence of any longitudinal pressure gradient, the classical electrokinetic velocity profile will be constant across the capillary cross-section and equal to the Smoluchowski slip velocity. This produces a net flow rate of

$$Q_E(\zeta) = u_{\text{EOF}} \pi a^2 \quad (2)$$

in the capillary with radius  $a$ .

However, if  $\zeta$ , varies along the capillary,  $Q_E$  would also vary longitudinally. This violates the law of mass conservation in compressible kinematics for unidirectional capillary flow, which stipulates that the steady-state flow rate must not vary down the capillary. The only alternative is that an additional opposing flow develops in regions with

large  $\zeta$  to reduce the local flow rate. This opposing flow is attributed to development of a longitudinal pressure gradient. Before steady state is established, the transient fast flowing regions slow down as this back pressure develops.

It is important to note that, according to this theory, the equilibrated flow rate with local pressure gradients, is specified by the EOF rate of the point with the lowest  $\zeta$  potential,  $Q = Q_E(\zeta_{\min})$ . In other words, the velocity profile remains, flat at the point of lowest  $\zeta$  potential, but everywhere else in the capillary, with  $\zeta > \zeta_{\min}$ , a pressure gradient develops such that the profile now becomes parabolic with a center-axis velocity opposite from the local wall velocity,  $u_{EOF}$ . Please refer to Fig. 7 for clarification.

Since the  $\zeta$  potential decrease at the anode due to the a drop in the pH, it is the anode end that determines the steady flow rate for the entire capillary while the remaining capillary retains the original zeta potential and slip velocity at the wall. The net flow flux through the capillary is specified by this area of highest resistance and is constrained to be uniform throughout the capillary due to mass balance kinematics. The pH in the anode well can sometimes drop below the isoelectric point of approximately pH 3 for

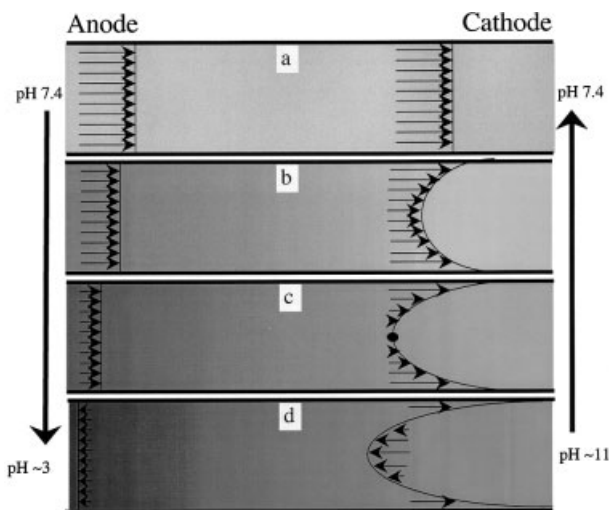


**Figure 7.** Two-dimensional flow profiles showing development of pressure driven back flow opposing the EOF in a capillary. (a) Classic electroendosmotic flat velocity profile determined by the Smoluchowski slip velocity at the capillary wall. (b) Zeta potential begins to drop at the anode end of the capillary. A pressure-driven backflow develops in the region of high zeta potential. Flow rate is controlled by the  $\zeta_{\min}(\text{anode})$  region of the capillary. (c) Pressure driven back flow increases to the point where the center axis velocity is zero (●). At this point,  $\zeta_{\min}(\text{anode}) = 0.5 \zeta_{\max}(\text{cathode})$ . (d) Anode end surpasses the isoelectric point and EOF is now toward the anode.  $\zeta_{\max}$  is still the same and a large back flow is present.

silica [14]. This means the charge on the capillary wall changes from negative to positive, completely reversing the zeta potential and the direction of EOF. The high resistance remains the controlling factor, even if the  $\zeta$  potential at the anode end changes sign, providing its absolute value is still smaller than that at the rest of the capillary. Here, we will treat the case where surface charge, and thus  $\zeta$  potential become small, but do not change sign.

This peculiar flow rate selection mechanism of a capillary with a longitudinal gradient in the  $\zeta$  potential can be quantified. Solution of the unidirectional Navier-Stokes equation in a cylindrical capillary with boundary condition (1) and with a constant pressure gradient yields the parabolic velocity profile

$$u(r) = \frac{1}{4\mu} \frac{\partial P}{\partial z} (r^2 - a^2) + u_{EOF}(\zeta) \quad (3)$$

with a corresponding flow rate or

$$Q = -\frac{\pi a^4}{8\mu} \frac{\partial P}{\partial z} + \pi a^2 u_{EOF}(\zeta) \quad (4)$$

Hence, the selected flow rate occurs when the pressure gradient is nonexistent.

$$Q_{\min} = \pi a^2 u_{EOF}(\zeta_{\min}) \quad (5)$$

The local pressure gradient that is established at every longitudinal location with  $\zeta > \zeta_{\min}$  can then be determined.

$$\frac{\partial P}{\partial z} = \frac{8\mu}{a^2} [u_{EOF}(\zeta) - u_{EOF}(\zeta_{\min})] \quad (6)$$

The center-axis velocity ( $r = 0$ ) at each location in the capillary with  $\zeta$  zeta potential is then a case of (3)

$$u(0) = 2u_{EOF}(\zeta_{\min}) - u_{EOF}(\zeta) \quad (7)$$

Consequently, the center-axis velocity changes sign when  $u_{EOF}(\zeta_{\min}) \leq 0.5 u_{EOF}(\zeta)$

Since  $u_{EOF}$  is proportional to  $\zeta$  from (1), one finds

$$\zeta_{\min} \leq \frac{\zeta}{2} \quad (8)$$

Therefore, a center-axis liquid velocity in the opposite direction is expected whenever the  $\zeta$  potential at the anode drops below half of its original value or half of the maximum value anywhere else in the capillary.

However, even when (8) is established and opposite flowing streamlines exist in the capillary, the net flow,  $Q_{\min}$ , still constrains the flow in the original direction. The opposite-flowing streamlines are continuous with EOF near the capillary wall to form recirculations (see Fig. 7). This changes slightly when the anode end reaches the isoelectric pH for silica. In this case,  $\zeta_{\min}$  changes sign and net flow,  $Q_{\min}$ , actually reverses sign.

The above arguments pertain to liquid flow only. The experimentally observed velocities are a combination of electroendosmotic flow and electrophoretic motion.

$$U_{\text{RBC, apparent}}(r) = u(r) + u_{\text{EP}}(\zeta_{\text{RBC}}) \quad (9)$$

Since the pH is lowest at the anode end of the capillary, the capillary zeta potential is lowest there and so is the electroendosmotic velocity. As a result, the velocity profile is expected to be flat at the anode by the above arguments (Fig. 7). RBC transport will then reverse if this EOF towards the cathode at the anode is smaller in magnitude than the electrophoretic velocity towards the anode. This would occur at a pH lower than the EOF reversal of (8) but at a pH higher than the isolectric pH of the capillary. This is outlined conceptually in Fig. 8. We offer an estimate of this critical pH below by estimating the zeta potentials of both the capillary and RBC.

Mobilities and zeta potentials for RBC are available in the literature [5, 17] for similar ionic conditions. For fresh RBC in phosphate buffer solution at pH 7.4, the electrophoretic mobility toward the anode is  $-1.60 \pm 0.05 \mu\text{m}\cdot\text{cm}/\text{Vs}$ . Table 1 estimates what the resulting electrophoretic velocities (calculated from Zukoski's  $\zeta$  value [5]) would be compared with observed RBC electrokinetic velocities in the electric fields currently employed. This estimate assumes the RBC is a sphere with a radius much larger than the Debye length such that the Smoluchowski electroendosmotic relation (1) can be used for electrophoretic velocity also. However, the apparent velocity estimate (9) assumes the RBC is much smaller than the capillary radius. Both are approximations that are difficult to correct theoretically.

Examination of the data in Table 1 and (9) show that the electroendosmotic velocity is about 1.5 times the electrophoretic velocity but is in the opposite direction. This is represented in the  $\zeta$  potential schematics of Fig. 8. The neutral zeta potential of the capillary is  $\sim 1.5$  times larger

**Table 1.** Electrophoretic velocities of RBCs compared to observed electrokinetic RBC velocities (all values are approximate)

Voltage (V/cm)	$\mu_{\text{EP}}$ ( $\mu\text{m/s}$ )	$U_{\text{RBC, apparent}}$ ( $\mu\text{m/s}$ )
12.5	$-20 \pm 0.63$	$\sim 11$
25	$-40 \pm 1.3$	$\sim 21$
37.5	$-60 \pm 1.9$	$\sim 30$
50	$-80 \pm 2.5$	$\sim 41$

The EOF velocity must be about 1.5 times the EP velocity of erythrocytes (Eq. 9) to produce the apparent RBC velocities that are half the bulk EP velocities.

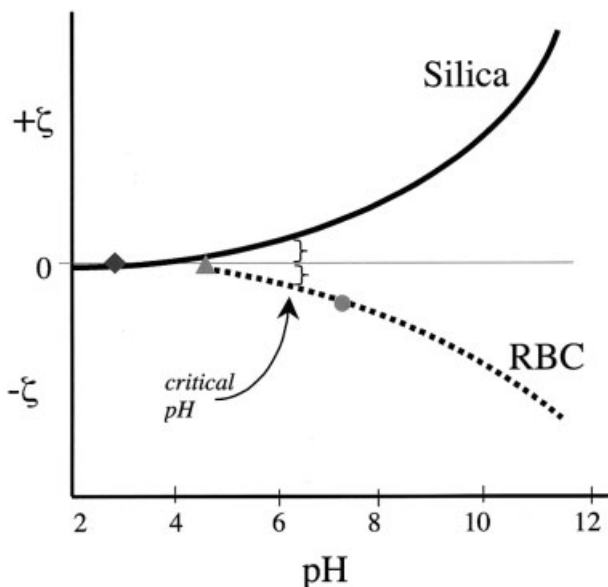


**Figure 8.** Qualitative schematic of zeta potentials of the silica wall and of erythrocytes as a function of pH. Isoelectric point of silica is approximately pH 3 (◆) [14]. (●) Zeta potential of a RBC is known at pH 7.4 [5] and (▲) at the isoelectric point of pH 4.2 [16]. The dotted line represents the hypothetical behavior of  $\zeta_{\text{RBC}}$  in PBS. The observed velocity is zero when the electrostatic force caused by the wall is equal and opposite to the electrostatic force the RBC exerts. Flow reversal is observed past this transition point of approximately pH 6.

in magnitude than the RBC zeta potential at neutral pH. The exact values will be estimated subsequently. However, one expects both zeta potentials to decrease with decreasing pH such that an isoelectric point of the capillary is reached at a pH of 3 from Bolt's measurements [14], and the isoelectric point of a RBC is reached at a pH of 4.2 from [17]. However, by extrapolating from the values in Fig. 8, we estimate a critical pH of about 6. This value requires an estimate of the capillary zeta potential as a function of pH, which is detailed below. At this critical pH value, the zeta potential is lower than that in (8) and significant pressure-driven back flow exists. However, the capillary zeta potential is still positive and the critical pH is above the capillary isoelectric point in Fig. 8. This critical pH is in rough agreement with our experimental observation for 37.5 V/cm.

Isotonic phosphate buffer solution is a simple salt solution containing NaCl,  $\text{KH}_2\text{PO}_4$ ,  $\text{K}_2\text{HPO}_4$  at the following concentrations:  $[\text{NaCl}] = 0.140 \text{ M}$ ;  $[\text{KH}_2\text{PO}_4] = 0.02498 \text{ M}$ ;  $[\text{K}_2\text{HPO}_4] = 0.00907 \text{ M}$ . Individual ion concentrations can be tabulated as follows assuming only the first ion in the phosphate complexes dissociates. These ions are in such low concentrations, they contribute very little to the total

ionic strength. The concentration of  $H^+$  is determined directly from the pH.  $[Na^+] = [Cl^-] = 0.140 \text{ M}$ ;  $[K^+] = 0.03405 \text{ M}$ ;  $[H_2PO_4^-] = 0.02498 \text{ M}$ ;  $[KHPO_4^-] = 0.00907 \text{ M}$ ;  $[H^+] = 10^{-\text{pH}}$ .

Using these ionic concentrations, the Grahame equation allows the surface charge density of the silica capillary surface to be related to the zeta potential [17]. To find the total ion concentration at the surface, which has a charge density of  $\sigma$ , a solution of the Poisson-Boltzmann equation can be employed as follows. See Israelachvili for boundary conditions and clarification [17].

$$\sum_i \rho_{oi} = \sum_i \rho_{\infty i} \frac{\sigma^2}{2\epsilon_0 kT} \quad (10)$$

where  $\rho_{oi}$  and  $\rho_{\infty i}$  represent each ion concentration at the surface and in the bulk, respectively.  $\epsilon$  is the dielectric permittivity index of water, while  $\epsilon_0$  is the permittivity of free space,  $k$  is the Boltzmann constant and  $T$  is the temperature, in this case ambient. The distribution of ions at the surface is dependent on the bulk electrolyte solution and can be estimated using the following expression:

$$\rho_{oi} = \rho_{\infty i} e^{-\frac{z_i e \zeta_0}{kT}} \quad (11)$$

where  $z_i$  is the charge of each ion in solution and  $e$  is the electron charge at  $1.602 \times 10^{-19} \text{ C}$ . Combining the expressions for each ion allows one to obtain an expression for the surface charge density in terms of the zeta potential. A simplification can be made if the zeta potential is expected to be below approximately 25 mV and is given by:

$$\sigma = \epsilon \epsilon_0 \kappa \zeta \quad (12)$$

where  $\kappa$  is the inverse of the Debye length and is given by the following:

$$\kappa = \left( \sum_i \frac{\rho_{\infty i} e^2 z_i^2}{\epsilon \epsilon_0 k T} \right)^{0.5} \text{ m}^{-1} \quad (13)$$

This expression is used to calculate the zeta potential from literature values of surface charge density. In 1957, Bolt [14] measured the adsorption isotherms of ions on a silica sol as a function of pH for a NaCl electrolyte. Since the dominant salt in PBS is NaCl, we use his charge density data in our  $\zeta$  potential estimates. Bolt's data shows the surface charge density for a wide range of concentrations of  $H^+$  ions, and is indicative of surface charge densities on the capillary wall. The surface charge of the fused-silica capillary in contact with the PBS solution at any pH can be found with the following expression:

$$\sigma = \frac{1.63095 C^2}{Jm^2} (0.3481 + 10^{-\text{pH}}) \zeta \quad (14)$$

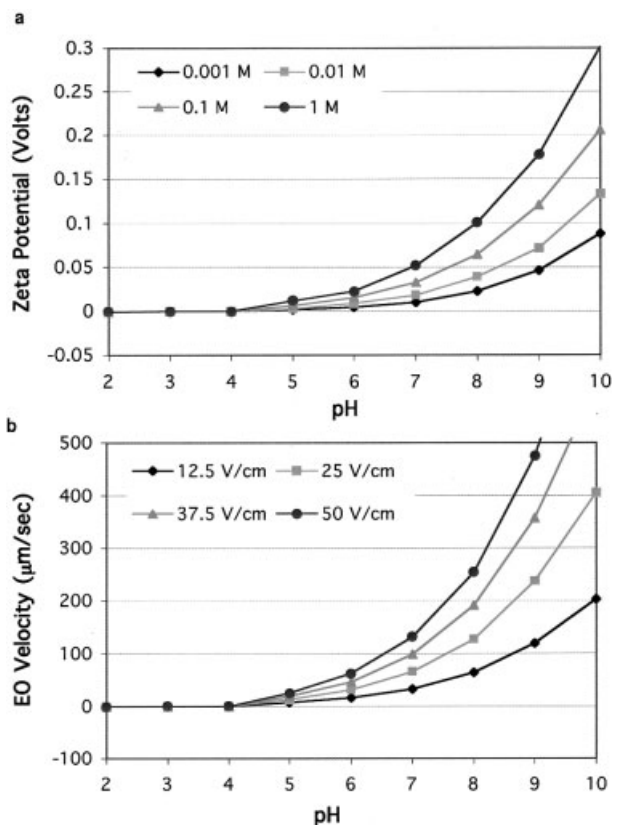


**Figure 9.** (a) Zeta potentials of the silica surface as a function of pH. Different symbols represent electrolyte concentrations from 0.001 to 1 M. PBS is on the order of 0.01 M. This was calculated using the simplified Grahame equation from Bolt's surface charge density data [14]. (b) Electroendosmotic velocities predicted by these  $\zeta$  potentials via the Smoluchowski relation. Different symbols represent the calculated values for electric fields of 12.5, 25, 37.5, and 50 V/cm.

Figure 9a shows zeta potentials calculated from this expression with surface charge data obtained from Bolt [14]. Utilizing the Smoluchowski relation, predicted electroendosmotic velocities are obtained as shown in Fig. 9b. The 25 V/cm data for capillary zeta potential are transferred to Fig. 10. Some RBC  $\zeta$  potential measurements were performed by Riddick [18], so in Fig. 10, we compare his measurements performed in a suspending medium of 5% sucrose to our computed silica zeta potentials. Riddick's value at neutral pH varies significantly from that obtained by Zukoski [5]. This can be accounted for with the difference in support media; sucrose is a far larger molecule than any of the salts found in PBS and alters the zeta potential of the RBC. While the numbers are different, the general trend is consistent with our theory shown schematically in Fig. 8.

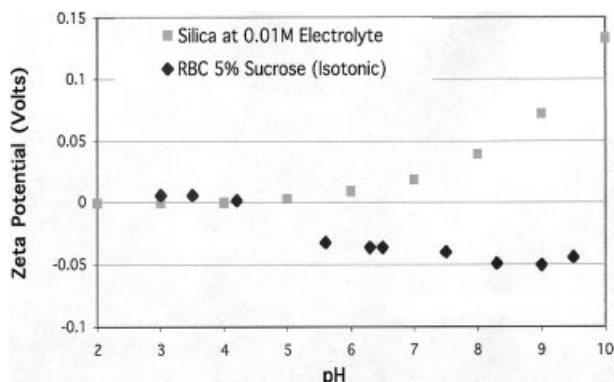


**Figure 10.** The pH dependence of an erythrocyte zeta potential ( $\blacklozenge$ ) in 5% sucrose by Riddick [18]. Zeta potentials for silica ( $\blacksquare$ ) are calculated using the Grahame relation from Bolt's data [14]. The data are similar to the qualitative estimates made in Fig. 7.

If microfluidic systems are to become commonplace in the lab, they need to utilize small scales and produce efficient and reliable results. Small volumes and reservoirs lead to ionic limitations in the sense that the few ions available are easily rearranged to produce pH gradients, zeta potential changes, and build-up of voltages. All of these characteristics will lead to several anomalous effects we have observed – settling of RBC within the capillary during slow EOF, cell aggregation into clusters at comers due to enhanced electric fields and flow reversal once a pH gradient develops.

We have removed settling and cell aggregation by increasing the electric field beyond 25 V/cm and have obtained preliminary evidence that a pH gradient due to an electrolysis reaction is responsible for the flow reversal, RBC reversal, and excess  $H^+$  at the anode. We have provided a theoretical justification of the flow reversal in light of changing zeta potentials due to the developing pH gradient. This link between the pH gradient between the wells and the changes in local zeta potentials is made through silica surface charge data [14] and the Grahame equation [17]. A simple experimental solution to the pH gradient is to precipitate the excess protons with a salt. This we have done at fields less than 12.5 V/cm by adding  $MgCl_2$ . However, significant electroendoosmotic velocity and pH polarization may be inevitable to transport RBC in capillaries smaller than 100  $\mu m$ . This may impose a lower limit on the dimensions of electrokinetic microdevices suitable for erythrocyte applications. One solution is, of course, to use a disposable device whose pH is never

lower than the critical pH of 6 we estimate. This design constraint would require an additional, careful estimate of the RBC zeta potential to replace the Riddick data of Fig. 10. Further careful experiments are currently underway in our laboratory to resolve these difficulties and to move microdevices for medical applications forward.

The authors would like to thank Kristen King for performing the pH experiments and Tyler Schmidt for help with the data acquisition board and LABVIEW programming. Research expenses are supported by NSF XYZ-on-a-Chip (Grant #CTS99-80745). Graduate stipend support is provided by the Clare Booth Luce Fellowship Fund.

Received January 8, 2002

## 5 References

- [1] Stone, H. A., Kim, S., *AIChE J.* 2001, 47, 1250–1254.
- [2] Chang, H.-C., *Bubble/Drop Transport in Microchannels*, The MEMS Handbook, CRC Press, Boca Raton, FL 2001, pp. 11–1–11–13.
- [3] Takhistov, P., Indeikina, A., Chang, H.-C., *Phys. Fluids* 2002, 14.
- [4] Whitesides, G. M., Stroock, A. D., *Physics Today* 2001, 54, 42–48.
- [5] Zukoski, C. F., Saville, D. A., *J. Colloid Inter. Sci.* 1987, 115, 422–436.
- [6] Roberts, M. A., Locascio-Brown, L., MacCrehan, W. A., Durst, R. A., *Anal. Chem.* 1996, 68, 3434–3440.
- [7] Herr, A. E., Molho, J. I., Santiago, J. G., Mungal, M. G., Kenny, T. W., Gargiulo, M. G., *Anal. Chem.* 2000, 72, 1053–1057.
- [8] Tachev, K. D., Angarska, J. K., Danov, K. D., Kralchevsky, P. A., *Colloids Surfaces B: Biointerfaces* 2000, 19, 61–80.
- [9] Fahraeus, R., Lindqvist, T., *Am. J. Phys.* 1931, 96, 562–568.
- [10] Gupta, B. B., Seshadri, V., *Biorheology* 1977, 14, 133–143.
- [11] McKay, C. B., Meiselman, H. J., *Am. Phys. Soc.* 1988, 88, H238–H249.
- [12] Raisi, F., Belgrader, P., Borkholder, D. A., Herr, A. E., Kintz, G. J., Pourhamadi, F., Taylor, M. T., Northrup, M. A., *Electrophoresis* 2001, 22, 2291–2295.
- [13] Cabrera, C. R., Finlayson, B., Yager, P., *Anal. Chem.* 2001, 73, 658–666.
- [14] Bolt, G. H., *Phys. Chem.* 1957, 61, 1166–1169.
- [15] Takeuchi, M., Miyamoto, H., Sako, Y., Komizu, H., Kusumi, A., *Biophys. J.* 1998, 74, 2171–2183.
- [16] Duginov, K., Takhistov, P., Chang, H.-C., in preparation.
- [17] Israelachvili, J., *Intermolecular and Surface Forces*, Academic Press, San Diego, CA 1992, pp. 213–254.
- [18] Riddick, T. M., *Control of Colloid Stability through Zeta Potential*, Wynnewood, PA, Published for Zeta-Meter, by Livingston Pub. Co., Wynnewood, PA 1968.